ORIGINAL RESEARCH

Tobacco Mosaic Viral Nanoparticle Inhibited Osteoclastogenesis Through Inhibiting mTOR/ AKT Signaling

Zhongshu Shan[1,2,*]
Hongtao Bi [ID][3,*]
Angxiu Suonan[2]
Yong Gu[1]
Huan Zhou[4]
Kun Xi[1]
Rui Xiong[5]
Hua Chen[2]
Liang Chen[1]

[1]Department of Orthopedic Surgery, The 1st Affiliated Hospital of Soochow University, Suzhou, Jiangsu, People's Republic of China; [2]Department of Orthopedic Surgery, People's Hospital of Qinghai Province, Xining, Qinghai, People's Republic of China; [3]Qinghai Provincial Key Laboratory of Tibetan Medicine Pharmacology and Safety Evaluation, Northwest Institute of Plateau Biology, Chinese Academy of Sciences, Xining, Qinghai, People's Republic of China; [4]Department of Radiography, Rocket Army Specialty Medical Center, Beijing, People's Republic of China; [5]Nutrition Department, People's Hospital of Qinghai Province, Xining, Qinghai, People's Republic of China

*These authors contributed equally to this work

Correspondence: Liang Chen
Department of Orthopedic Surgery, The 1st Affiliated Hospital of Soochow University, 188 Shizi St. Suzhou, Jiangsu 215006, People's Republic of China
Email chenliangspine@163.com

Introduction: Tobacco mosaic virus-based nanoparticles (TMV VNPs) were previously shown to promote osteogenic differentiation in vitro. This study aims to investigate whether and how TMV VNPs impact on osteoclastogenesis in vitro and bone injury healing in vivo.
Methods: Raw264.7 cells were cultured in osteoclastogenic medium in culture plates coated with or without TMV and TMV-RGD1 VNPs, followed by TRAP staining, RT-qPCR and WB assessing expression of osteoclastogenic marker genes, and immunofluorescence assessing NF-κB activation. TMV and TMV-RGD1-modified hyaluronic acid hydrogel were used to treat mouse tibial bone injury. Bone injury healing was checked by micro-CT and Masson staining.
Results: TMV and TMV-RGD1 VNPs significantly inhibited osteoclast differentiation and downregulated the expression of osteoclastogenic marker genes Ctr, Ctsk, Mmp-9, Rank, and Trap. Moreover, TMV and TMV-RGD1 VNPs inhibited NF-κB p65 phosphorylation and nuclear translocation, as well as activation of mTOR/AKT signaling pathway. TMV and TMV-RGD1-modified HA hydrogel strongly promoted mouse tibial bone injury with increased bone mass compared to plain HA hydrogel. The amount of osteoclasts was significantly reduced in TMV and TMV-RGD1 treated mice. TMV-RGD1 was more effective than TMV in inhibiting osteoclast differentiation and promoting bone injury repair.
Discussion: These data demonstrated the great potential of TMV VNPs to be developed into biomaterial for bone injury repair or replacement.
Keywords: tobacco mosaic virus, viral nanoparticle, osteoclast, mTOR, tibial bone injury

Introduction

Virus-based nanoparticles have been shown great potentials in biomedical applications such as drug delivery system,[1] imaging probe,[2] and biosensor.[3] Plant viral nanoparticles (VNPs) provide many advantages in terms of safety and bioavailability over other widely studied nanoparticles including liposomes, inorganic, and polymeric nanoparticles.[4] A large amount of empty non-infectious capsids of plant virus can be easily and rapidly produced using plants, which can be easily scaled up.[5] Tobacco mosaic virus (TMV) is rod-shaped with a length of 300 nm and a diameter of 18 nm. The rigid helical capsid of TMV is assembled with 2130 identical coat protein subunits.[6] Wild type and RGD1 mutant TMV nanoparticles have been shown to promote osteogenic differentiation of human bone marrow stem cells.[7,8]

Bone generation or repair is a dynamic process involving osteogenesis and osteoclastogenesis. Whereas osteoblasts and osteocytes participate in the new bone formation and mineralization bone organic matrix,[9,10] Osteoclasts are responsible for bone

resorption to remove old bone matrix.[10] Polyethylene-like nanoparticles and milk-derived nanoparticles could promote the formation of osteoclasts[11,12] while TMV-based nanoparticles were shown to be osteogenic.[7,8] This study aims to investigate whether and how TMV-base nanoparticles impact the differentiation of osteoclasts in vitro and in vivo.

Materials and Methods
Reagents

Soluble recombinant mouse RANKL and M-CSF were purchased from R&D (R&D Systems, Minneapolis, MN, United States). Tartrate-resistant acid phosphatase (TRAP) Kit was obtained from Sigma-Aldrich (St. Louis, MO, United States). Masson Kit was obtained from Solarbio (Beijing, China). Raw264.7 cells were purchased from CTCC.

Virus Preparation

Wild-type TMV (TMV) and its RGD1 mutant (TMV-RGD) (gifts from Dr. Qian Wang of the University of South Carolina) and isolated from infected tobacco leaves following previously established protocols.[13] Briefly, infected leaves were frozen to −80°C in Ziploc bags (~100−150 g of leaves per bag), crushed by hand, and transferred to a 1.5-liter blender. About 3 volumes of phosphate buffer with 0.2−0.3% 2-mercaptoethanol were added to the crushed leaves, blended for 2 min at low speed and then 3 min at the highest speed. The plant blend was filtered through two layers of cheesecloth and centrifuged 30 min at 13,500 rpm at 4°C. The supernatant was mixed with n-butanol and chloroform at 2:1:1 ratio, stirred for 30 min on ice, and centrifuged at 12,500 rpm for 20 min at 4°C. 0.2 M NaCl and 8% (wt/vol) PEG-8000 were added in after the aqueous layer was transferred to a beaker, mixed on ice for 60 min and centrifuged at 13,500 rpm for 20 min. The precipitated virus washed with 10 mM potassium phosphate buffer (pH 7) supplemented with 10 μg/mL PMSF and aliquoted and stored at −20°C.

Virus-Functionalized HA Hydrogel

Wild type and RGD1 mutant TMV1cys were generated following a previously published method[14] by adding a single cysteine residue (TGT codon) at the third position within the coat protein open reading frame using a PCR-based mutagenesis procedure. Infectious RNA transcripts generated from the TMV1cys cDNA clones were inoculated on Nicotiana tabacum, cv Xanthi to produce virus.

TMV-based HA hydrogels were made by dissolving HA (47 kDa) at 5 wt% concentration in a phosphate buffer saline solution (PBS), adding TMV1cys in phosphate buffer to a final concentration of 0.1 wt%, and mixing in dithiothreitol (DTT) at a molar ratio of thiol:ene = 1:4. HA only hydrogel was gelated without adding virus solution.

CCK-8 Assay

Raw264.7 cell proliferation in 0.1 mg/mL polyd-lysine (TCP) only or with an additional coating of 0.7 mL of 1 mg/mL TMV or TMV-RGD1 coated plates was measured by Cell Counting Kit-8 (C0038, Beyotime Biotech, Shanghai, China). 5000 Raw264.7 cells in 200 μL medium was added into 96 well plate and cultured at 37°C for 24 h. 20 μL of CCK-8 solution was added into each well and incubated at 37°C for 1 h before read at 450 nm on a microplate reader (Molecular Device, San Jose, CA).

Raw264.7 Cell Attachment Assay

5000 Raw264.7 cells in 200 μL medium were seeded in 0.1 mg/mL polyd-lysine (TCP) only or with additional coating of 0.7 mL of 1 mg/mL TMV or TMV-RGD1 coated 96-well plates. After 1 h culture at 37°C, medium was removed and the unattached cells were removed by carefully washing twice with PBS. 100 μL medium was added and the cells were photographed and counted.

In vitro Osteoclastogenesis Assay

Raw264.7 cells were cultured in DMEM low glucose medium containing 10% FBS, 2mM Glutamine, and penicillin-streptomycin mixture until the number is enough on the packaged plate, respectively. 2, 5, and 7 days after RANKL (50 ng/mL) treatment, TRAP staining was carried out according to the manufacturer's instructions for osteoclasts detection.

Immunofluorescence Staining

The effects of TMV and TMV-RGD1 on the nuclear translocation of NF-κB p65 were determined by immunofluorescence as previously described. Cells were fixed with 4% paraformaldehyde for 15 min, washed with 0.2% Triton X-100 in PBS for 10 min, blocked with 1% BSA in PBS, and incubated with monoclonal anti-P65 antibody (Abcam, Cambridge, MA, USA) followed by biotinylated goat anti-mouse IgG antibody (Abcam) and fluorescein-conjugated streptavidin (Vector Laboratories, Burlingame, CA, USA). Cells were counterstained with propidium iodide (Vector Laboratories).

7144

International Journal of Nanomedicine 2020:15

The Effects on P65 Expression

Raw264.7 cells were evaluated by Western blotting. The Raw264.7 cells were seeded (2–3×10^6 cells/well) into 6-well plates which packaged TMV and its RGD mutant. Cells were evaluated by Western blotting to observe P65 (1:350, Santa Cruz, sc-398,442), phosphorylation of P65 (1:500, Santa Cruz, sc-136,548) and GAPDH (1:200, Santa Cruz, sc-32,233).

Quantitative Real-Time Polymerase Chain Reaction (qPCR)

Total RNA was extracted from cells tissues using RNeasy mini kits (Qiagen, Venlo, Netherlands). Reverse transcription was performed with the SuperScript$^®$ III First-Strand Synthesis System (Life Tech, Shanghai, China) according to the supplier's instructions using 1 g total RNA. Quantitative real-time PCR was performed using the SYBR$^®$ Green PCR Master Mix (Life Tech) on an ABI 7300 (Applied Biosystems, Foster City, CA) according to the manufacturer's recommendation with the following program: 95°C for 10 min followed by 40 cycles of 95°C for 20 sec, 62°C for 20 sec, and 72°C for 30 sec. The expression of purpose gene was normalized to GAPDH. All experiments were done triplicate. The $2^{-\Delta\Delta Ct}$ method was used to calculate the relative expression of genes. The primers used were TGACACAGCAGAAAAGGT and GCCAGGTAATAAA GAACG for Ctr, CAGGGTCCCAGACTCCAT and CGC CTCCACAGCCATAAT for Ctsk, CCCTGTGTGTTCCC GTTC and TCCTGGTCATAGTTGGCT for Mmp9, GCT ATGGGGCTGCTTGTT and GGGTGGCATTGGGTCTTC for Trap, ATCCAGCAGGGAAGCAAA and GGGACACG GGCATAGAGT for Rank, GGTGAAGGTCGGTGTGAA CG and CTCGCTCCTGGAAGATGGTG and for GAPDH. The relative transcription levels were calculated with the $2^{-\Delta\Delta Ct}$ method using GAPDH as the internal control.

The Expression of p-S6K

The cells were fixed with 4% paraformaldehyde for 20 min, permeabilized with 0.1% Triton X-100 in PBS for 15 min, and blocked in 10% normal goat serum for 1 h at room temperature. The cell was then incubated with p-S6K (1:100, Cell signaling, 9204S) at 4°C overnight and then with Cy3-conjugated Affinipure Goat Anti-Rabbit IgG(H+L) secondary antibodies (SA00009-2, Proteintech, China) and Fluorescein isothiocyanate-conjugated F-actin antibodies (1:100, Abcam, ab205) were used to detect F-actin.

Animals and Experimental Design

The animal protocol was approved by the Institutional Animal Care and Use Committee of People's Hospital of Qinghai Province. All experiments strictly followed the protocol and the Regulations on Laboratory Animal Welfare issued by Chinese Ministry of Science and Technology. 8-week old mice were purchased from Cavens (Changzhou, China). Twenty-four rats were randomly divided into Model, HA, HA-TMV and HA-TMV-RGD group with six rats in each group. The animal model was tibial bone injury model, and rats were anesthetized, and hair was removed from the left hind limb. An incision was made in the skin over the medial aspect of the proximal tibia. Soft tissue was cleared from the distal end of the tibial crest, and a hole (1 mm in diameter) that penetrated through both lateral cortices and the intervening medulla was created in the bone using a 19-gauge needle attached to an electric drill. HA hydrogel was carefully placed in the defect, the periosteum was repositioned, and skin incision was closed with a continuous suture. Mice were sacrificed with the approved protocol and tibia bones were harvested 7 days after injury.

Tissue Collection

Left hind limbs were dissected and fixed overnight in 4% paraformaldehyde at 4°C. Bones for histologic analysis were decalcified for at least 2 weeks in 14% ethylenedia-minetetraacetic acid (EDTA; Sigma), pH 7.2. Once decalcified, all specimens were processed for paraffin embedding using a Shandon Pathcenter Processor (Thermo Electron Corporation, Waltham, MA, USA). Bones for micro-computed tomographic (μCT) analysis were placed in 69% ethanol following fixation.

Paraffin Embedding and Histological Analysis

The treated tissue was wrapped in paraffin to prepare paraffin sections (section thickness of 5um). Masson staining analysis was carried out by selecting better quality sections.

Bone Structure Analysis

The tibial tissue was analyzed using micro-computed tomography (Micro CT, Skyscan1172, Antwerp, Belgium). The analysis conditions were 80, 124 μA and resolution was 8 μm. Structural parameters for skull were analyzed using the built-in software. Total bone mineral density (BMD) was measured, and the trabecular parameters were evaluated as the bone volume/total volume (BV/TV), trabecular number

(Tb. N), trabecular pattern factor (Tb. Pf), bone surface area expressed per unit total volume (BS/TV). Two-dimensional and three-dimensional bone structure image slices were reconstructed.

Statistical Analysis

The data were expressed as mean ± standard deviation. The differences between groups were analyzed by one-way Analysis of Variance using Graphpad Prism 5 and Origin 6.1. A p value less than 0.05 was considered statistically significant.

Results
TMV-Based Nanoparticles Promoted Osteoclastogenesis

To evaluate the potential effect of TMV VNPs on the differentiation of osteoclasts, Raw264.7 mouse macrophages were induced with RANKL in plates coated with 0.1 mg/mL polyd-lysine (TCP) only or with an additional coating of 0.7 mL of 1 mg/mL TMV or TMV-RGD1.[8]

TMV and TMV-RGD1 did not have any effect on the proliferation (Figure 1A) and attachment (Figure 1B and C) of Raw264.7 cells. However, TMV and TMV-RGD1 coating promoted the flattening and forming fibroblast shape by Raw264.7 cells (Figure 1B). Compared to TCP, TMV and TMV-RGD1 significantly delayed osteoclast differentiation and reduced the number of osteoclasts (Figure 2A). Meanwhile, the mRNA (Figure 2B) and/or protein (Figure 2C) levels of osteoclastogenesis genes NFATc1 and RANK and osteoclast markers Ctr, Ctsk, Mmp-9, and Trap were markedly downregulated by TMV and TMV-RGD1 VNPs. The inhibitory effect of TMV-RGD1 was more prominent than that of TMV (Figure 2).

TMV VNPs Inhibited Osteoclastogenesis by Blocking the Activation of NF-κB Pathway

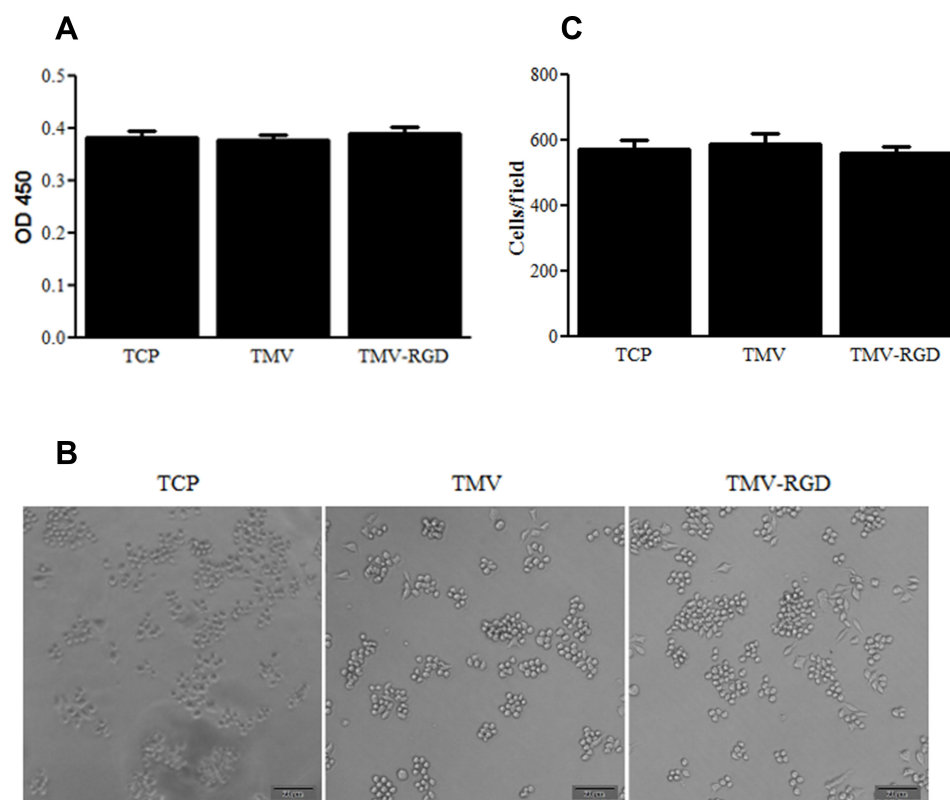As TMV VNPs were able to inhibit osteoclastogenesis, we next examined whether they had any impact on the

Figure 1 TMV VNPs did not influence the proliferation and attachment of Raw264.7 cells. (**A**). Raw264.7 cells were cultured 96 well plate coated with 0.1 mg/mL polyd-lysine (TCP) only or with additional coating of 0.7 mL of 1 mg/mL TMV or TMV-RGD1 for 24 h and then assessed with CCK-8 assay. (**B**). Raw264.7 cells were cultured 96 well plate coated with 0.1 mg/mL polyd-lysine (TCP) only or with additional coating of 0.7 mL of 1 mg/mL TMV or TMV-RGD1 for 1 h and unattached cells were then removed. The attached cells were photographed and representative pictures were shown. (**C**). The number of average cells per field from 10 random fields was shown.
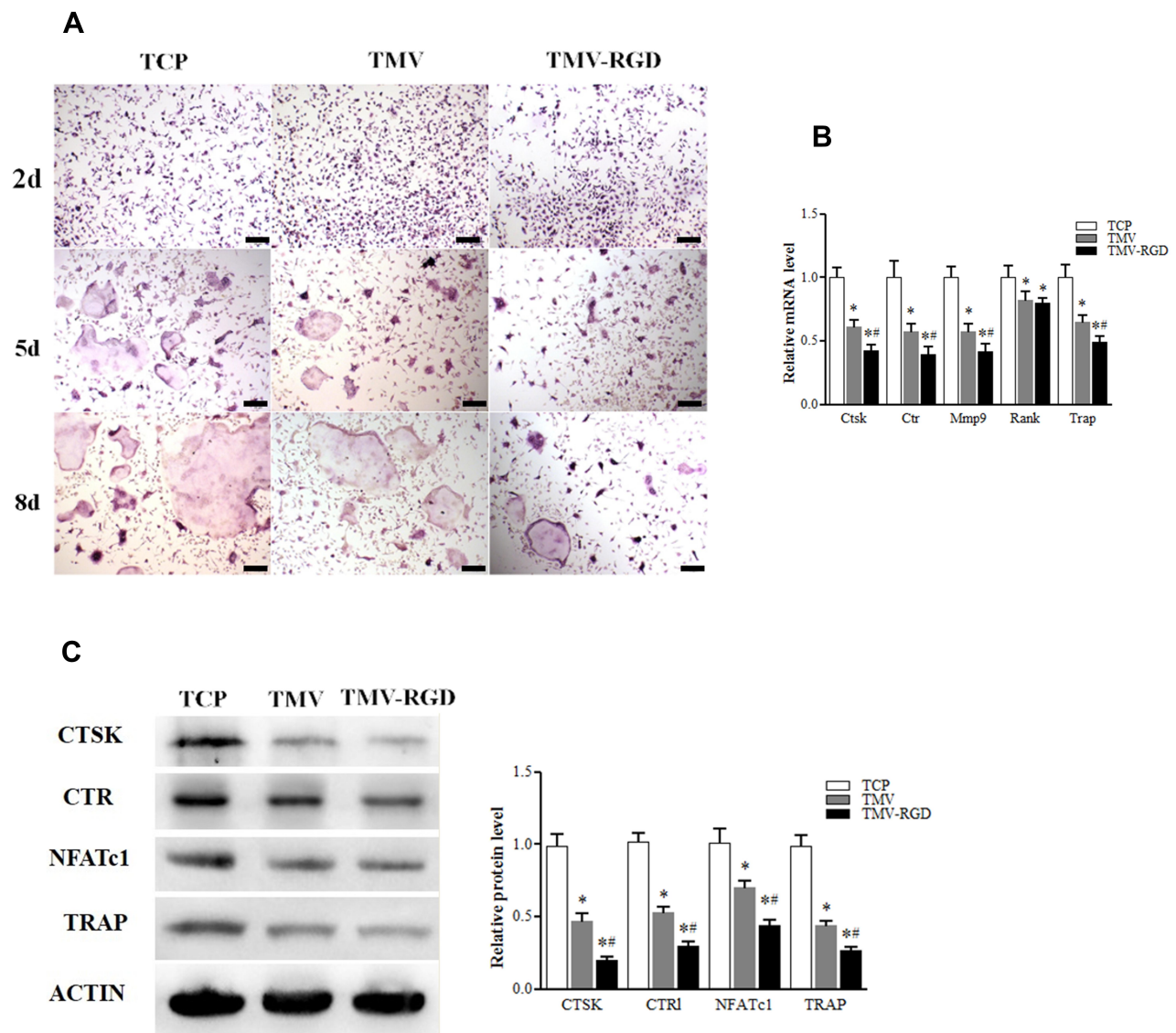
Figure 2 TMV VNPs inhibited osteoclastenesis. (**A**). Raw264.7 cells were treated with 50 ng/mL RANKL in specified plates for 2, 5, and 7 days before TRAP staining to show the effects of TMV and TMV-RGD1 VNPs on osteoclast differentiation. (**B**). Raw264.7 cells were treated with 50 ng/mL RANKL in plates coated with or without TMV and TMV-RGD1 VNPs for 8 days and mRNA levels of Ctr, Rank, Ctsk, Trap, and Mmp-9 were assessed by real-time quantitative PCR. (**C**). The protein levels of CTSK, CTR, NFATc1, and TRAP of Raw264.7 treated with 50 ng/mL RANKL in plates with or without TMV and TMV-RGD1 VNPs for 8 days were analyzed by immunoblotting. *$p<0.05$ compared to TCP, #$p<0.05$ compared to TMV.

activation of NF-κB, which is indispensable for osteo-clast differentiation. Western blot showed that the phosphorylation of NF-κB p65 was substantially inhibited by TMV and TMV-RGD1 VNPs. Moreover, the inhibition of NF-κB p65 phosphorylation by TMV-RGD1 was more severe than that by TMV (Figure 3A). After 24 h RANKL treatment, NF-κB p65 was mostly located in the nuclear of Raw264.7 cells cultured in bare tissue culture plates but mainly distributed in the cytoplasm of cells cultured in TMV and TMV-RGD1 coated plates (Figure 3B).

TMV VNPs Promoted Bone Injury Healing

We next investigated whether TMV VNPs could impact the healing process of bone injuries using a rat tibia injury model. TMV and TMV-RGD1 VNPs functionalized HA hydrogel (Figure 4A) was used to fill the injuries. A week later, cancellous bone started to form from the rim of the injury in mice without any treatment (Figure 4B). The injury of mice treated with HA hydrogel was covered with a thin layer of cancellous bone whereas mice treated with TMV and TMV-RGD1 functionalized HA hydrogel were completely healed with cortical bone (Figure 4B). Masson
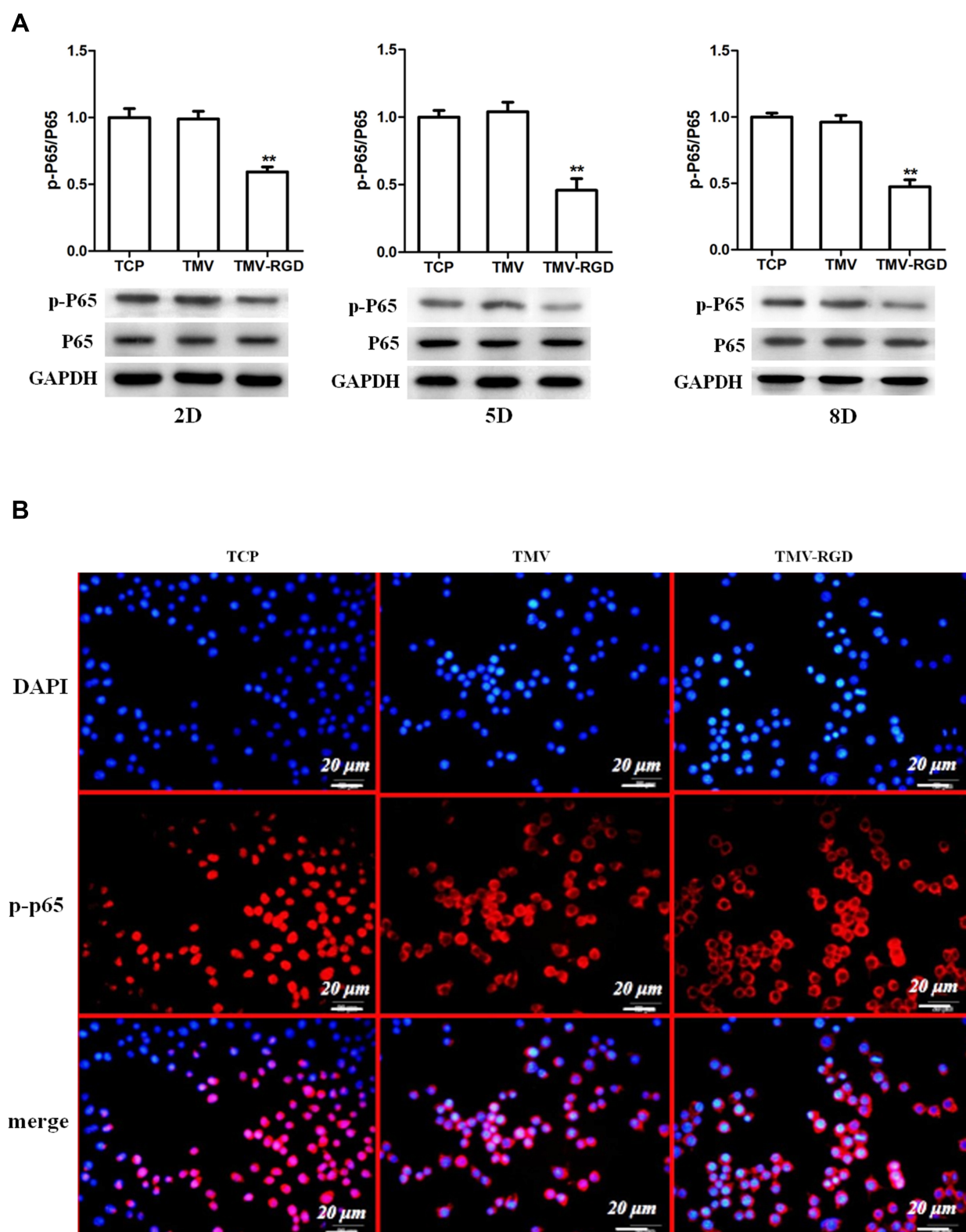
A

B

Figure 3 TMV VNPs inhibited NF-κB activation. (**A**). Phosphorylation of NF-kB p65 at different time of osteoclast differentiation was evaluated by immunoblotting. (**B**). The cellular localization of NF-κB p65 of Raw264.7 cells was assessed by immunocytofluorescence 24 h after RANKL (50 ng/mL) treatment. NF-κB p65 of cells cultured in naked plates mostly located in nuclear while that of cells in TMV and TMV-RGD coated plates mostly resided in cytoplasm. **p<0.01 compared to TCP.

staining confirmed that cancellous bone appeared around the parameter of the injury in mice without treatment. HA hydrogel treated mice had both cancellous bone and cortical bone at injury site, while the bone at the injury site of mice treated with TMV- and TMV-RGD1 functionalized HA hydrogel were completely mineralized (Figure 4C). Consistently, HA hydrogel and TMV- and TMV-RGD1 functionalized HA hydrogel increasingly augmented local bone volume (Figure 4D), trabecular bone number (Figure 4E), and trabecular bone thickness (Figure 4F).

TMV VNPs Inhibited Osteoclast Differentiation During Tibial Injury Repair

Bone injury repair is essentially a regenerative process involving the change of balance between osteogenesis and osteoclastogenesis.[15] We then examined whether osteoblast and osteoclast differentiation peri-injury site was changed by TMV and TMV-RGD1 NPs. Compared to untreated or plain HA hydrogel treated mice, TMV and TMV-RGD1 functionalized HA hydrogel significantly reduced F4/80 positive osteoclast progenitor cells infiltrating into surrounding bone tissue of tibia injury (Figure 5A). Consistently, the amount of TRAP-positive osteoclasts were significantly decreased in injured bone tissue of rats treated with TMV or TMV-RGD1 functionalized HA hydrogel (Figure 5B).

TMV VNPs Inhibit Osteoclastogenesis via Inactivation of mTOR/Akt Pathway

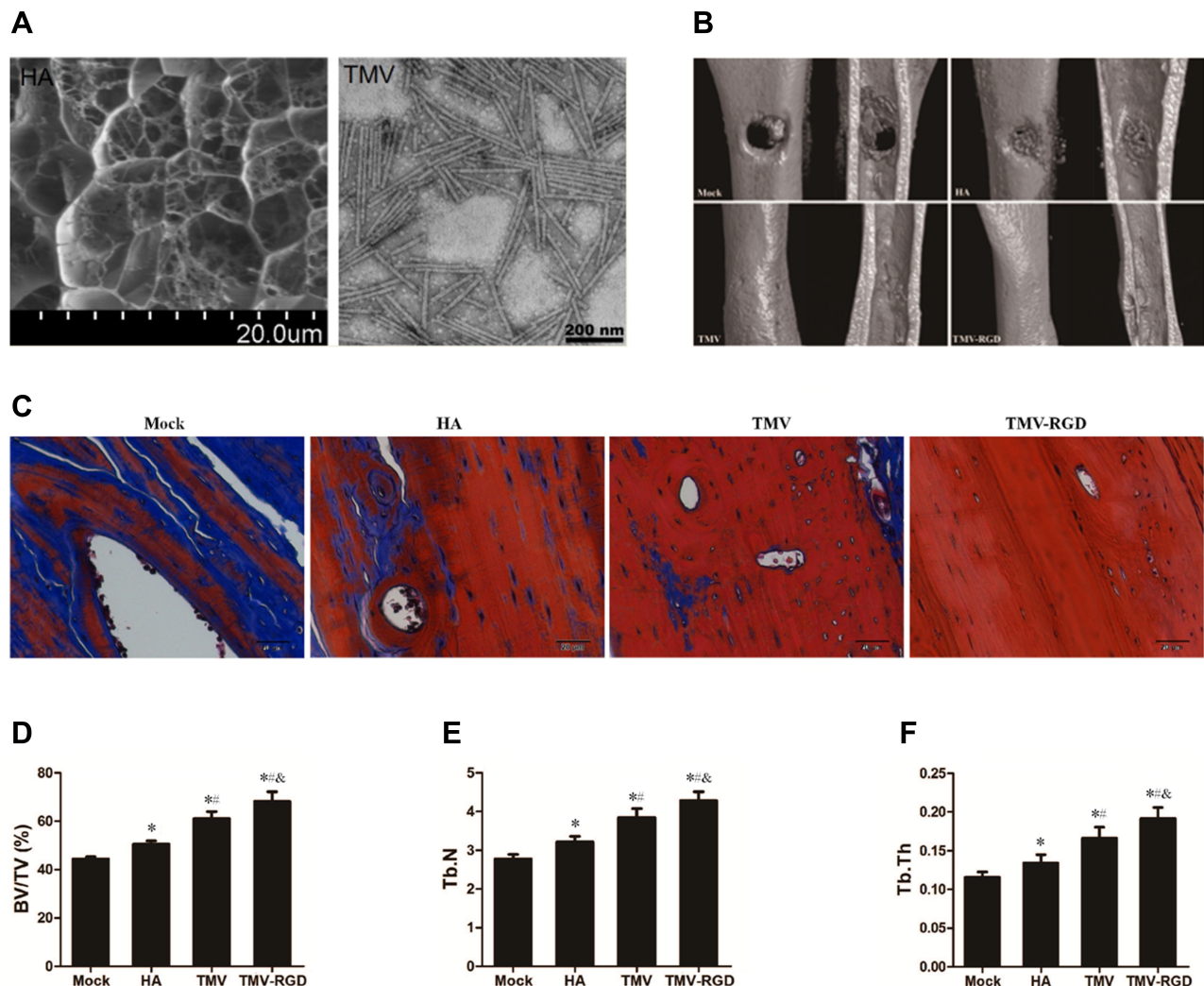It has been shown that mTOR-AKT signaling regulates osteoclastogenesis[16] so we next examined whether this

Figure 4 TMV VNPs improved healing of mouse tibia injury. (**A**) The morphology of HA hydrogel (left panel) and cross-linked TMV VNPs (right panel) was examined using scanning electron microscope. (**B**). Micro-CT images showed that TMV or TMV-RGD1 VNP-modified HA hydrogel accelerated healing of tibia injury. (**C**). Mouse tibial bone injury healing and mineralization were assessed by Masson staining. Local bone volume (**D**), trabecular bone number (**E**), and trabecular bone thickness (**F**) were all improved by TMV and TMV-RGD1. *$p<0.05$ compared to Mock, #$p<0.05$ compared to HA, &$p<0.05$ compared to TMV.
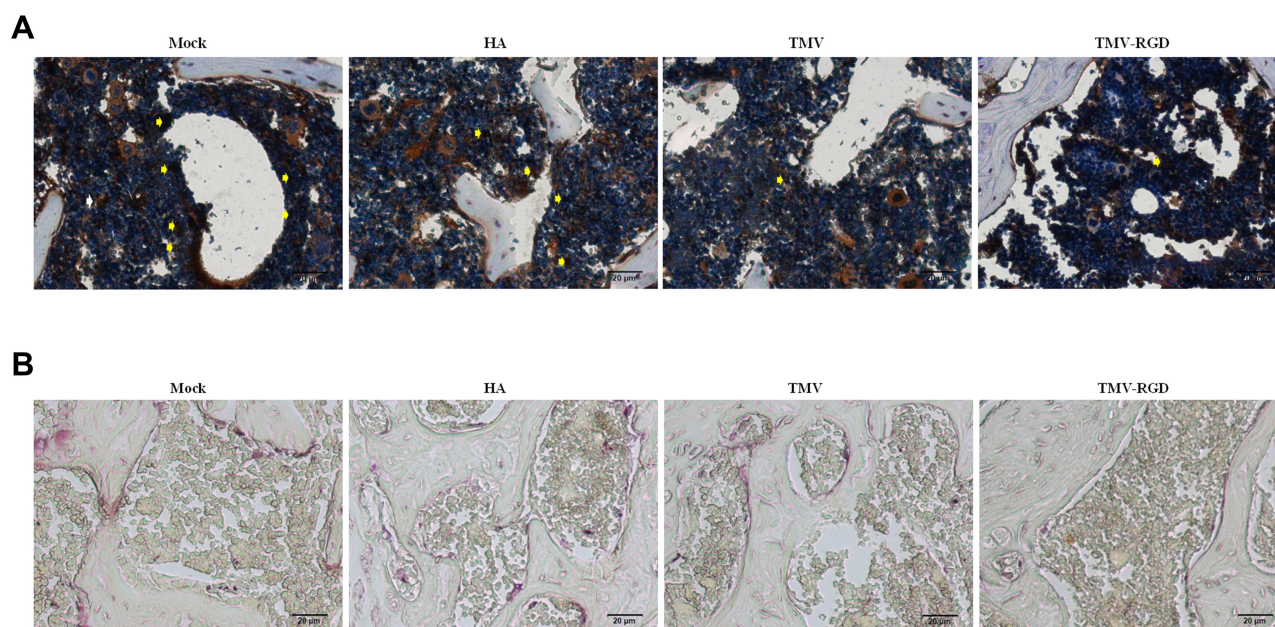
Figure 5 TMV VNPs inhibited osteoclast differentiation at injury site. (**A**). TMV and TMV-RGD modified hydrogel reduced infiltration of F4/80-positive macrophages into tibial injury sites as shown by immunohistochemical staining. (**B**). TRAP-positive osteoclasts were significantly less in tibial bone treated with TMV and TMV-RGD modified hydrogel.

signaling pathway was impacted by TMV and TMV-RGD1 VNPs. The phosphorylation of mTOR (Figure 6A) and its downstream target p70 S6K (Figure 6B) were significantly decreased in Raw264.7 cells cultured in TMV or TMV-RGD1 coated plates. Moreover, Akt phosphorylation was also inhibited by TMV or TMV-RGD1 coating (Figure 6C). The inhibition of mTOR-AKT activation by TMV-RGD1 VNPs was significantly stronger than that by TMV VNPs (Figure 6AC). Raw264.7 macrophages cultured in naked culture plates differentiated into osteoclasts (F-actin rings) and the phosphorylated S6K level was markedly increased after RANKL treatment, which was markedly suppressed by TMV and TMV-RGD1 VNPs coating (Figure 6D). Furthermore, S6K phosphorylation in injured tibial bone tissue was substantially reduced in TMV and TMV-RGD1 functionalized HA hydrogel treated mice compared to plain HA hydrogel treated mice (Figure 6E).

Discussion

The current study demonstrated that TMV-based viral nanoparticles were effective in inhibiting osteoclastogenesis both in vitro and in vivo. RGD1 mutant TMV VNPs were more potent in inhibiting osteoclast differentiation of Raw264.7 cells, phosphorylation and nuclear translocation of NF-κB p65, activation of mTOR/Akt signaling pathway in vitro. TMV and TMV-RGD1 VNPs modified HA

hydrogel promoted healing of mouse tibial bone injury through inhibiting osteoclastogenesis. TMV and TMV-RGD1 VNPs markedly suppressed mTOR signaling in injured tibial bone tissues.

TMV VNPs promoted osteoblast differentiation of rat bone marrow stem cells on aminopropyltriethoxysilane coated glass slides, during which TMV augmented the upregulation of osteogenic genes and reduced the time required for osteoblast induction by about a week.[17] Phosphate modified TMV was more potent in osteogenic induction than wild-type TMV on both aminopropyl-triethoxysilane coated and titanium coated glass slides.[18] TMV and its RGD1 mutant enhanced osteogenic differentiation of human bone marrow stem cells on polyd-lysine-coated cell culture plates with augmented expression of osteogenic marker genes including Runx2, osteocalcin, and osteopontin.[8] The osteoinductive effect of TMV might root from its ability to induce the overexpression of bone morphogenetic protein 2 at early phase.[19] Potato virus X (PVX) engineered to present mineralization-inducing (MIP) and RGD peptides on the surface of PVX VNPs enhanced cell adhesion, osteoblast differentiation, and mineralization in vitro.[20] The common theme of these studies was that plant VNP-modified materials could strongly promote osteoinduction in vitro. However, there has been a lack of investigation on how would these
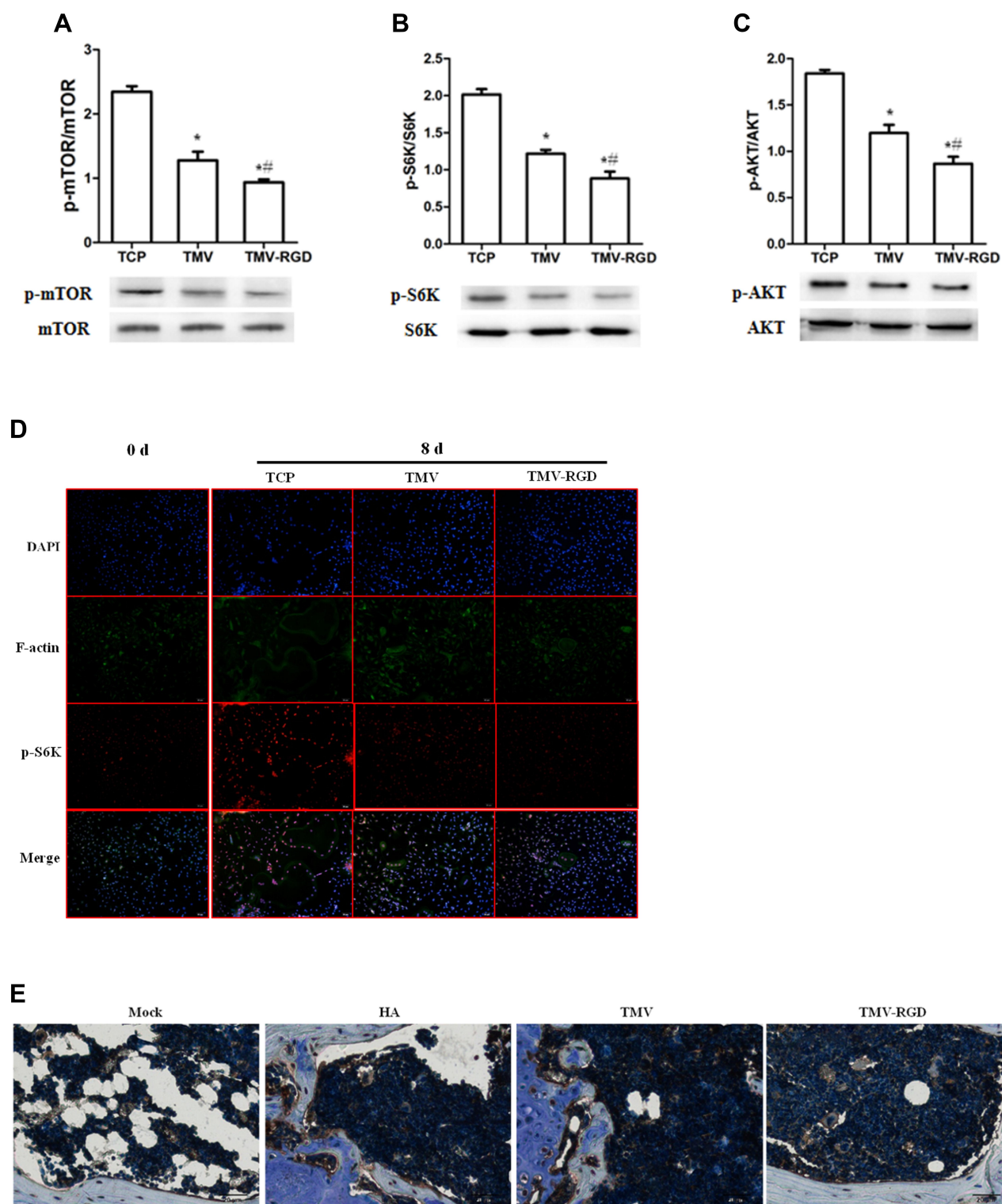
Figure 6 TMV VNPs inhibited mTOR/AKT signaling. Phosphorylation of mTOR (**A**), p70 S6K (**B**), and AKT (**C**) in Raw264.7 cultured in osteoclast differentiation medium in naked plates or TMV and TMV-RGD1 coated plates was assessed by immunoblotting. (**D**). F-actin and p-S6K of Raw264.7 osteoclast induction for 8 days in naked plates or TMV and TMV-RGD coated plates were visualized with immunocytofluorescence. (**E**). Levels of p-S6K at mouse tibial bone injury site was evaluated by immunohistochemistry. *p<0.05 compared to TCP; #p<0.05 compared to TMV.

materials perform in vivo and whether they could impact osteoclastogenesis.

This study aimed to explore whether TMV viral nanoparticles could impact osteoclast differentiation as different nanoparticles were shown to modulate osteoclastogenesis.[11,12,21–25] Gold nanoparticle (GNP) was one of the well-studied inorganic nanoparticles on osteoclastogenesis.[21–23] β-cyclodextrin (CD) conjugated GNPs carrying curcumin and alendronate functionalized GNPs inhibited RANKL-induced mouse bone marrow-derived macrophages differentiation into tartrate-resistant acid phosphatase (TRAP)-positive multinuclear osteoclasts and the expression of osteoclastogenic genes c-Fos, Nfatc1, Trap, and Oscar in vitro and improved bone density of ovariectomized mice.[21,22] Nanoparticles derived from milk increased the number of small osteoclasts (≤5 nuclei) but did not change the bone resorptive activity both in vitro and in vivo.[12] Bioactive glass nanoparticles promoted adhesion to culture plate surface and osteoclast differentiation of Raw264.7 cells, which was accompanied by the upregulation of Ctsk, Ca2, Ror2, Syncytin-A/B, and Trap5a/b.[24] Polyethylene-like nanoparticles were readily internalized by human macrophages and osteoclasts and promoted osteoclastogenesis.[11] Ultra-high molecular weight polyethylene wear particles promoted inflammatory responses and osteoclastogenesis of Raw264.7 cells with elevated expression of osteoclast markers MMP-9, Calcr, and Ctsk.[25] These data showed that a variety of nanoparticles could change the course of osteoclast differentiation, which inspired the current study to investigate the impact of TMV VNPs on osteoclastogenesis in vitro and on bone injury healing in vivo.

Rapamycin was shown to cause significant reductions in osteoclast numbers, size, and nucleation in a dose-dependent manner whereas Akt inhibition resulted in marked reduction in osteoclast number but not as effective in osteoclast size and nucleation.[16] Osteoprotegerin upregulated the expression of autophagy-related proteins, reduced tartrate-resistant acid phosphatase-positive osteoclast number and bone resorption activity, and inhibited AMPK/mTOR/p70S6K signaling pathway.[26] Deletion of Raptor (inactivation of mTORC1) with Ctsk promoter-driven Cre recombinase resulted in less TRAP-positive osteoclasts and increased bone density and volume.[27] Moreover, AKT was shown to act downstream of mTOR to regulate osteoclast differentiation.[16] Hydrogen sulphide promoted osteoclast differentiation by inhibiting autophagy through the activation of mTOR/AKT signaling.[16]

AKT phosphorylated IKK protein to activate NF-κB and promote the epithelial–mesenchymal transition and migration of osteosarcoma MG-63 cells.[28] Taken together, TMV and TMV-RGD1 nanoparticles blocked RANKL-induced activation of mTOR/AKT/NF-κB signaling pathway, led to inhibition of osteoclast differentiation.

In conclusion, TMV and TNV-RGD1 VNPs strongly inhibited osteoclast differentiation of Raw264.7 macrophages. The expression levels of osteoclastogenic marker genes Ctr, Ctsk, Mmp-9, Rank, and Trap were significantly suppressed by TMV and TNV-RGD1VNPs. Moreover, TMV VNPs blocked the activation of mTOR/Akt signaling pathway and inhibited the phosphorylation and nuclear translocation of NF-κB p65 protein. TMV and TNV-RGD1 VNPs functionalized HA hydrogel promoted the healing of tibial bone injury by inhibiting osteoclast differentiation. These data demonstrated that TMV and TMV-RGD1 VNPs could be used to functionalize currently used biomaterials to enhance their bone repair ability.

Disclosure
The authors report no conflicts of interest for this work.

References
1. Bruckman MA, Czapar AE, Steinmetz NF. *Drug-Loaded Plant-Virus Based Nanoparticles for Cancer Drug Delivery." Virus-Derived Nanoparticles for Advanced Technologies*. New York, NY: Humana Press; 2018:425–436.
2. Wojta-Stremayr D, Pickl WF. Fluorosomes: fluorescent virus-like nanoparticles that represent a convenient tool to visualize receptor-ligand interactions. *Sensors*. 2013;13(7):8722–8749. doi:10.3390/s130708722
3. Lebedev N, et al. A virus-based nanoplasmonic structure as a surface-enhanced Raman biosensor. *Biosens Bioelectron*. 2016;77:306–314. doi:10.1016/j.bios.2015.09.032
4. Pokorski JK, Steinmetz NF. The art of engineering viral nanoparticles Mol. *Pharmaceutics*. 2011;8:29–43.
5. Love AJ, et al. The use of tobacco mosaic virus and cowpea mosaic virus for the production of novel metal nanomaterials. *Virology*. 2014;449:133–139. doi:10.1016/j.virol.2013.11.002
6. Clare DK, Orlova EV. 4.6 Å cryo-EM reconstruction of tobacco mosaic virus from images recorded at 300 keV on a 4k× 4k CCD camera. *J Struct Biol*. 2010;171(3):303–308. doi:10.1016/j.jsb.2010.06.011

7. Andrew LL, et al. Multivalent ligand displayed on plant virus induces rapid onset of bone differentiation. *Mol Pharm*. 2012;9 (7):2121–2125. doi:10.1021/mp300042t

8. Liu T, et al. Using plant virus based nanorods to modulate the differentiation of human bone marrow stem cells. *J Biomed Nanotechnol*. 2019;15(2):363–372. doi:10.1166/jbn.2019.2691

9. Xiao W, et al. *Cellular and Molecular Aspects of Bone Remodeling." Tooth Movement*. Vol. 18. Karger Publishers; 2016:9–16

10. Kaur S, et al. Role of bone marrow macrophages in controlling home-ostasis and repair in bone and bone marrow niches. *Seminars Cell Develop Biolo*. 2017;61:12–21. doi:10.1016/j.semcdb.2016.08.009

11. Brulefert K, et al. Pro-osteoclastic in vitro effect of Polyethylene-like nanoparticles: involvement in the pathogenesis of implant aseptic loosening. *J Biomed Mater Res A*. 2016;104(11):2649–2657. doi:10.1002/jbm.a.35803

12. Oliveira MC, et al. Milk-derived nanoparticle fraction promotes the formation of small osteoclasts but reduces bone resorption. *J Cell Physiol*. 2017;232(1):225–233. doi:10.1002/jcp.25414

13. Andrew LL, et al. Mutant plant viruses with cell binding motifs provide differential adhesion strengths and morphologies. *Biomacromolecules*. 2012;13(2):422–431. doi:10.1021/bm2014558

14. Maturavongsadit P, et al. Promotion of in vitro chondrogenesis of mesenchymal stem cells using in situ hyaluronic hydrogel functiona-lized with rod-like viral nanoparticles. *Biomacromolecules*. 2016;17 (6):1930–1938. doi:10.1021/acs.biomac.5b01577

15. Majidinia M, et al. The roles of signaling pathways in bone repair and regeneration. *J Cell Physiol*. 2018;233(4):2937–2948. doi:10.1002/jcp.26042

16. Tiedemann K, et al. Regulation of osteoclast growth and fusion by mTOR/raptor and mTOR/rictor/Akt. *Frontiers Cell Develop Biol*. 2017;5:54. doi:10.3389/fcell.2017.00054

17. Kaur G, et al. Regulation of osteogenic differentiation of rat bone marrow stromal cells on 2D nanorod substrates. *Biomaterials*. 2010;31(7):1732–1741. doi:10.1016/j.biomaterials.2009.11.041

18. Kaur G, et al. The synergistic effects of multivalent ligand display and nanotopography on osteogenic differentiation of rat bone marrow stem cells. *Biomaterials*. 2010;31(22):5813–5824. doi:10.1016/j.biomaterials.2010.04.017

19. Sitasuwan P, et al. A plant virus substrate induces early upregulation of BMP2 for rapid bone formation. *Integrative Biol*. 2012;4 (6):651–660. doi:10.1039/c2ib20041d

20. Lauria I, et al. Engineered Potato virus X nanoparticles support hydroxyapatite nucleation for improved bone tissue replacement. *Acta Biomater*. 2017;62:317–327. doi:10.1016/j.actbio.2017.08.039

21. Heo, Nyoung D, et al. Inhibition of osteoclast differentiation by gold nanoparticles functionalized with cyclodextrin curcumin complexes. *ACS Nano*. 2014;8(12):12049–12062. doi:10.1021/nn504329u

22. Lee D, et al. Inhibition of osteoclast differentiation and bone resorp-tion by bisphosphonate-conjugated gold nanoparticles. *Sci Rep*. 2016;6:27336. doi:10.1038/srep27336

23. Zeng L, et al. Au nanoparticles attenuate rankl-induced osteoclasto-genesis by suppressing pre-osteoclast fusion. *J Nanosci Nanotechnol*. 2019;19(4):2166–2173.

24. Detsch R, et al. Nanoscale bioactive glass activates osteoclastic differentiation of RAW 264.7 cells. *Nanomedicine*. 2016;11 (9):1093–1105. doi:10.2217/nnm.16.20

25. Cang D, Guo K, Zhao F. Dendritic cells enhance UHMWPE wear particle-induced osteoclast differentiation of macrophages. *J Biomed Mater Res A*. 2015;103(10):3349–3354. doi:10.1002/jbm.a.35459

26. Tong X, et al. Osteoprotegerin inhibit osteoclast differentiation and bone resorption by enhancing autophagy via AMPK/mTOR/p70S6K signaling pathway in vitro. *J Cell Biochem*. 2019;120(2):1630–1642. doi:10.1002/jcb.27468

27. Dai Q, et al. Inactivation of regulatory-associated protein of mTOR (Raptor)/mammalian target of rapamycin complex 1 (mTORC1) sig-naling in osteoclasts increases bone mass by inhibiting osteoclast differentiation in mice. *J Biol Chem*. 2017;292(1):196–204. doi:10.1074/jbc.M116.764761

28. Zhang X, et al. COX-2 promotes epithelial-mesenchymal transition and migration in osteosarcoma MG-63 cells via PI3K/AKT/NF-κB signaling. *Mol Med Rep*. 2019;20(4):3811–3819. doi:10.3892/mmr.2019.10598